

Multistatic Synthetic Aperture Imaging of Aircraft using Reflected Television Signals

Yong Wu and David C. Munson, Jr.

Coordinated Science Lab and Dept. of Electrical and Computer Engineering

University of Illinois at Urbana-Champaign, Urbana, IL 61801

email: yongwu@uiuc.edu, d-munson@uiuc.edu

ABSTRACT

We investigate passive radar imaging of aircraft using reflected TV signals. Such passive multistatic “radar” has been developed to detect and track aircraft with good accuracy. The additional capability of image formation would help to identify targets. The Fourier space sampling provided by passive radar is nonuniform. For a given aircraft flight path, different receiver locations give rise to different sampling patterns. We simulate multistatic radar returns using Fast Illinois Solver Code (FISC) and show that a good sampling pattern can be used to form a recognizable target image using direct Fourier reconstruction. However, a bad sampling pattern can make it impossible to form a useful image. In the Gaithersburg, MD area, we can select a good receiver location using 21 or fewer channels, which provides good enough Fourier-space coverage to form a useful aircraft image.

Keywords: Passive radar, SAR, image reconstruction from nonuniform data, point spread function

1. INTRODUCTION

Passive multistatic radar has been developed to detect and track aircraft using reflected TV signals.¹⁻⁴ This type of radar system could be useful in surveillance. The additional capability of image formation would help to identify aircraft. This is a multistatic synthetic aperture radar imaging problem. We assume one receiver, and many transmitters at different locations. As an aircraft traverses its flight path, the receiver collects TV signals reflected from the target. According to the bistatic radar principle, this data represents samples of the Fourier transform of the reflectivity of the target.^{5,6} Each narrow-band transmitter provides data on one arc in Fourier space. Multiple transmitters give multiple arcs. We investigate the feasibility of image formation by simulating multistatic radar returns at 211.25 MHz and below, using Fast Illinois Solver Code (FISC). Our simulations show that, by selecting a good receiver location, we can obtain a recognizable image of the aircraft. We expect the quality of the image to be even better if data is collected at higher frequencies (e.g. near 800 MHz). We also find that a bad receiver location can give sparse Fourier data and make successful imaging impossible. Therefore, for a given flight path, the receiver location is an important factor. We show how to select a good receiver location, which will give good Fourier-space coverage. Our study suggests that it is possible to produce recognizable aircraft images with passive radar, using 21 or fewer TV stations in the Gaithersburg, MD area.

2. MULTISTATIC SYNTHETIC APERTURE RADAR

In bistatic radar, the transmitter and receiver are spatially separated. The angle between the incident and observing direction is called the bistatic angle β . For monostatic radar, the bistatic angle is 0° . Figure 1 illustrates the bistatic radar configuration. Under certain assumptions, the data collected at transmitting frequency f is a sample of the Fourier transform of the target reflectivity and is equivalent to a monostatic measurement taken at the bisecting direction and at a frequency of $f \cos(\beta/2)$.^{5,6} As the receiver rotates away from the transmitter, the bistatic angle β increases and the equivalent frequency $f \cos(\beta/2)$ decreases. When β is 180° , the measurement is a sample located at the origin in Fourier space. Measurements collected from a receiver that rotates 360° around the target lie on a circle in Fourier space, passing through the origin. The diameter of the circle is $4\pi f/c$. Different incident frequencies give data on circles in Fourier space with different diameters, as shown in Fig. 1 (right). If the transmitter rotates around the target, the circle in Fourier space also rotates by the same amount and we get more circles of data in Fourier space. Fig. 1 (right) illustrates the type of Fourier space coverage obtained through angular and frequency diversity in a bistatic radar.

This work is supported by DARPA under the contract number F49620-98-1-0498

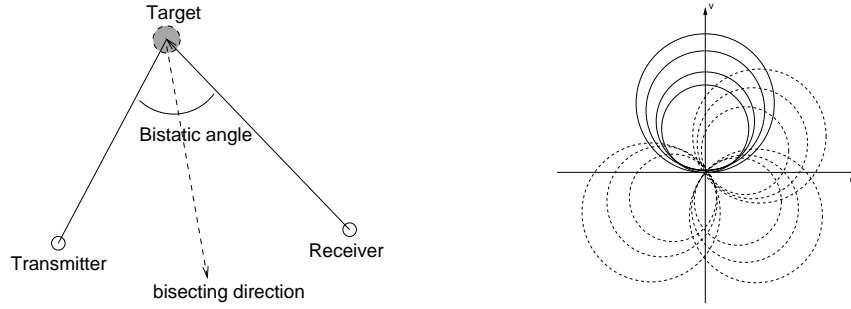


Figure 1. Left: bistatic radar configuration; Right: bistatic Fourier-space coverage due to angular and frequency diversity.

Multistatic radar is a system having multiple receivers and/or transmitters. The above bistatic principle applies to each transmitter/receiver pair. For each position of the target, transmitter and receiver, a single frequency signal from one transmitter/receiver pair provides Fourier data at a single point in Fourier space. In our passive radar scenario, there is one receiver and multiple transmitters. Fig. 2 illustrates a multistatic radar configuration. As the target moves, the bistatic angle and the bisecting direction change. Therefore the corresponding points in Fourier space will have both frequency and angular diversity. Different transmitters use different frequencies and are at different locations, which leads to multiple arcs of Fourier data, providing much further data diversity.

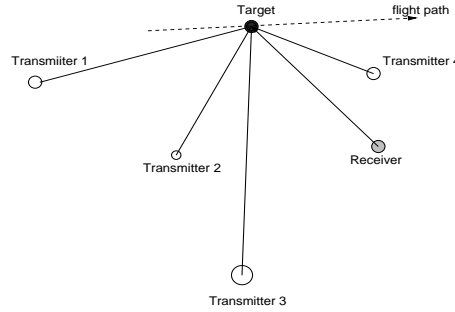


Figure 2. A multistatic radar configuration.

We consider a transmitter-receiver geometry for a passive radar system in the Gaithersburg, MD area. There are 37 TV stations scattered in this area. Figure. 3 gives a list of the channel numbers, frequencies and transmitter locations. The location is specified in km. For target detection and tracking, only 3 TV or radio channels are needed. In order to form images, however, we definitely need many more than 3 TV channels to provide good coverage in Fourier space. The data grid will be nonuniform. Denser data will help to reduce aliasing prior to image formation. Wider coverage in Fourier space potentially will yield a better point spread function (PSF) and improve the resolution of the image.

In the Gaithersburg area, TV transmitters are grouped in several locations. The amount of required receiving equipment and signal processing hardware increases with the number of TV stations used. From the 37 available, suppose we select 21. For each transmitter location, select a subset of the channels, from the highest frequency downward, with a minimum frequency spacing of 4 channels, or 24 MHz. The 21 channels could be selected as the following: No. 48, 42, 36, 32, 28, 20, 15 for transmitter location (20,10), No. 58 for (40,15), No. 64 and 51 for (30,15), No. 22 for (60,15), No. 63 for (70,15), No. 59, 52, 46, 40, 13 for (60,55), No. 67 for (50,65), No. 54, 41 and 24 for (50,50). Here, we have not selected any channel below 13, since higher frequencies are generally more helpful in providing high resolution. Fig. 4 shows the locations of the target, TV stations and receiver. The TV stations are located at (20, 10), (40, 15), (30, 15), (60, 15), (70, 15), (60, 55), (50, 55), the target is flying from (-40, -40) to (60, 110) in a straight line, and the receiver can be positioned anywhere within a rectangular area from (-30, -30)

Channel	Frequency (MHz)	Location (x,y)	Channel	Frequency (MHz)	Location (x,y)
2	55.25	(60,55)	38	614.25	(60,55)
4	67.25	(20,10)	39	620.25	(20,10)
5	73.25	(20,10)	40	626.25	(60,55)
7	175.25	(20,10)	41	632.25	(50,50)
9	187.25	(20,10)	42	638.25	(20,10)
11	199.25	(60,55)	45	656.25	(60,55)
13	211.25	(60,55)	46	662.25	(60,55)
14	470.25	(20,10)	48	674.25	(20,10)
15	476.25	(20,10)	50	686.25	(30,15)
20	506.25	(30,15)	51	692.25	(30,15)
22	518.25	(60,15)	52	698.25	(60,55)
24	530.25	(50,50)	54	710.25	(50,50)
26	542.25	(20,10)	58	734.25	(40,15)
28	554.25	(20,10)	59	740.25	(60,55)
30	566.25	(20,10)	61	752.25	(70,15)
32	578.25	(20,10)	63	764.25	(70,15)
34	590.25	(20,10)	64	770.25	(30,15)
35	596.25	(20,10)	67	788.25	(50,65)
36	602.25	(20,10)			

Figure 3. A list of TV channels, frequencies and the transmitter locations in Gaithersburg, MD area.

to (60, 60), where the coordinate unit represents km. Fig. 5 shows the nonuniform data grid in Fourier space using the selected 21 transmitters and a receiver location located at $(-30, -10)$. The Fourier space origin is at the central bottom of the figure. A semicircular region of the Fourier space is shown, with its radius equal to 8.76 radians/meter. As shown by simulation in next section, 21 channels can provide good coverage in Fourier space and give good image reconstruction. Using less channels will degrade the image quality. Obviously, there is a trade-off in the number of TV channels and the reconstructed image quality.

As mentioned earlier, higher frequencies are preferred in the above channel selection procedure, since they can yield image with higher resolution. We note that different transmitting locations offer different diversity in the Fourier space, so we selected some transmitters from each location. For some situations when the bistatic angle β is quite small, we might get sparse samples in Fourier space in the radial direction, since the channel spacing might be $\Delta f \cos(\beta/2) \approx \Delta f = 24$ MHz, which would not meet the Nyquist criterion for a large aircraft (a 6 MHz channel spacing will give the Nyquist coverage in Fourier space for an aircraft of length 15 m). For other situations when the bistatic angle β is large, the 'effective' frequency spacing between channels ($\Delta f \cos(\beta/2)$) might be much smaller than 24 MHz, therefore the radial spacing in Fourier space might be close to Nyquist spacing. This will ensure that the Fourier space data is sampled densely enough to provide for an accurate reconstruction.

3. IMAGE FORMATION SIMULATIONS

Passive multistatic radar imaging is similar to conventional synthetic aperture radar (SAR) imaging.^{7-9,6} To reconstruct the image of a target, we can interpolate the acquired Fourier data to a uniform rectangular grid and apply a 2D IFFT. This is called direct Fourier reconstruction (DFR). We note that the data available could be sparse

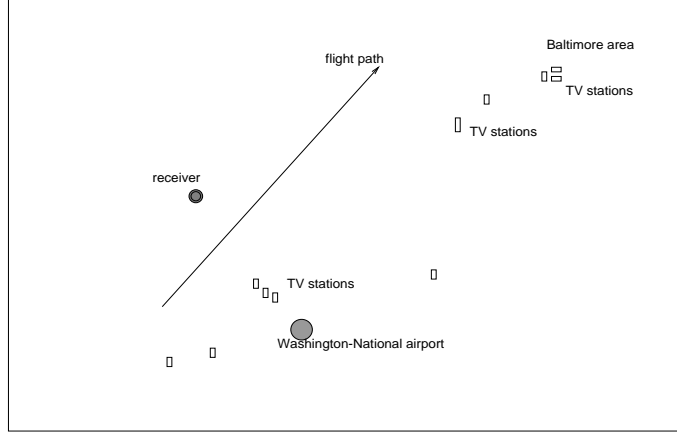


Figure 4. Receiver, transmitter location and target flight path

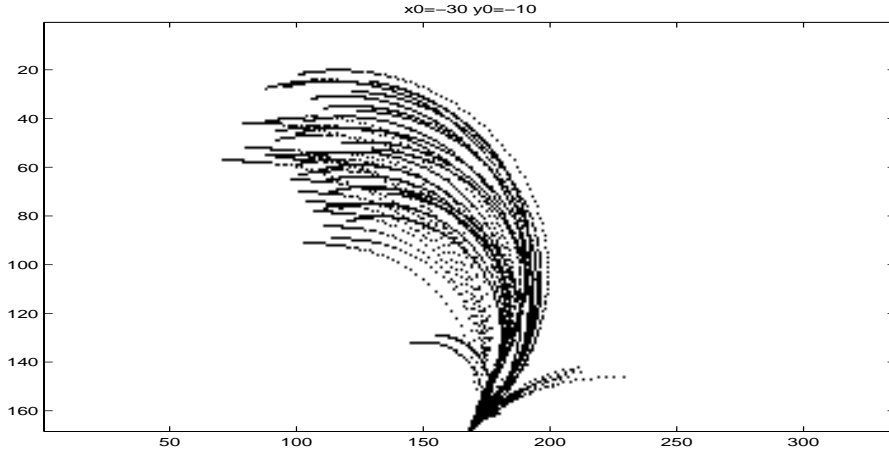


Figure 5. The nonuniform Fourier grid provided by 21 transmitters (for frequencies up to 800 MHz), receiver location at $(-30, -10)$.

in general. We used DFR to reconstruct the image in our simulations. Other methods, like the CLEAN algorithm, or other super-resolution methods could also be used to reconstruct images from the sparse data.

The problem of data interpolation from a nonuniform grid to a uniform grid has been studied in radio astronomy, medical imaging and geophysics. The gridding method is a popular approach to interpolate the nonuniform data to a Cartesian grid.¹⁰ Rasche has proposed calculating the Voronoi diagram of the sampling distribution and using it as a measure of the sampling density function in the convolution interpolation formula.¹¹ For simplicity, we used the Matlab interpolation function *griddata* to interpolate the data to a uniform grid. This algorithm is based on Delaunay triangulation.¹²

We simulate the multistatic radar returns using FISC. A Falcon-100 aircraft model is used in the simulation. Fig. 7 shows its optical image. Ideally we wished to generate data at the chosen 21 TV station frequencies to populate the Fourier grid in Fig. 5. However, it is computationally expensive to simulate data at high frequencies. For example, it may take months to simulate data at 800 MHz. Thus, we simplified our data generation. Instead of directly generating the data at the various station frequencies, we instead, as a first step, generated data on a complete grid as in Fig. 6 (right) using only the single frequency 211.25 MHz. For this data generation, we assumed 360 receivers around the target and one transmitter. The azimuth spacing between the receivers was 1° . The transmitter rotated around the target in a step of 5° . The total rotation was 180° . Fig. 6 (left) illustrates the experiment setup. For

each transmitter location, data collected by all receivers is mapped to a circle in the Fourier space passing through the origin, as shown in Fig. 6 (right). As the transmitter rotated 5° , the circle in Fourier space also rotated 5° . Therefore, after all rotations, the circles mapped out dense region in Fourier space.

We will now describe how this data set was used to mimic data from transmitters at multiple frequencies. Channel 5, 7, 9, 11, 13, 14, 20, 22, 24, 26, 30, 34, 38, 39, 41, 45, 48, 51, 58, 61, 67 are used in the simulation. The large box at the top of Fig. 8 shows the 21-channel Fourier data grid. Using FISC, we simulated the Fourier data only within a semicircular region within the smaller box shown at the top of Fig. 8. The grid inside the smaller box corresponds to the data that could be generated with a 211.25 MHz signal. The larger data grid would require frequencies up to 800 MHz. Since we were unable to generate the higher frequency data, our image reconstruction used only the data from the 21 channels that falls within the smaller box. All higher-frequency data was assumed to be zero. Thus, our simulations used only a small fraction of the data that would be available in practice from the 21 stations. As a result, the images that we present below provide a loose lower bound on the quality that could be expected from a real system. Fig. 8 also shows, in rows 2-5, 16 other Fourier data grids corresponding to a variety of receiver locations. We show only the parts of the Fourier grids that fall within our 211.25 MHz FISC data set (small box in top row). Notice that the 2-D sparsity of the Fourier grids varies considerably with receiver location.

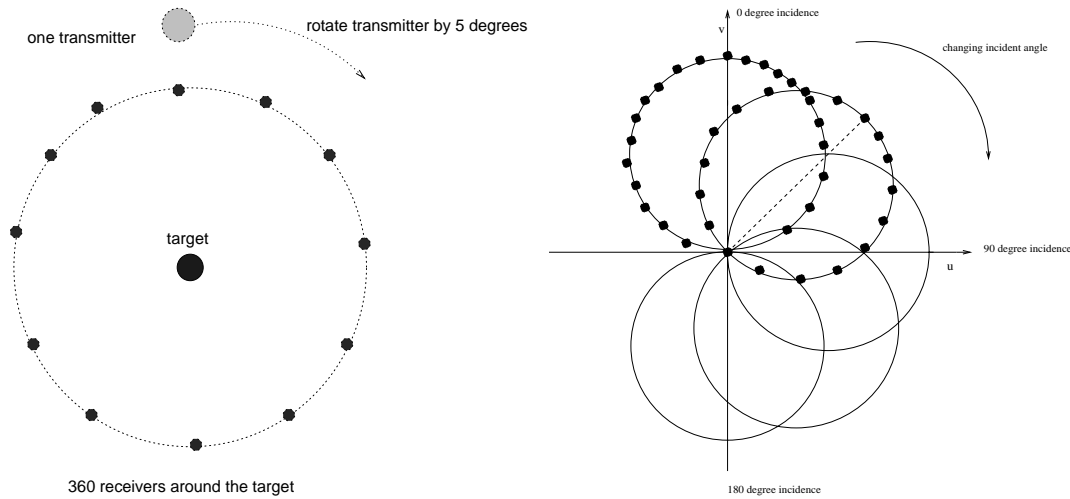


Figure 6. Left: Illustration of multistatic radar data collection. Right: Fourier space coverage of the FISC simulation



Figure 7. Optical image of Falcon-100

The Falcon-100 Fourier data on the nonuniform grid was interpolated to a uniform rectangular grid using the Matlab function *griddata* and then processed by a 2D IFFT to produce the reconstructed image. In Fig. 9, we show the interpolated Fourier data on uniform rectangular grids and the reconstructed images (second, third, fourth rows) for three different receiver locations, in comparison to the complete Fourier data and its image reconstruction (first

row). The spatial dimensions of the reconstructed image are 31.4 m by 31.4 m. The three Fourier patterns used were for receiver locations at $(-10, 50)$, $(-30, 50)$ and $(10, -10)$. The Fourier grids were shown in Fig. 8 (bottom left, third row and second column, bottom right of the figure, respectively). The first and second patterns give good image reconstructions, which are shown in the second and third rows of Fig. 9. Compared to the image obtained from complete dataset, these two images show the left wing clearly, and part of the right wing. The nose and tail also can be seen. In contrast, the third pattern provides sparse Fourier data and the reconstructed image (last row of Fig. 9) shows only the fuselage. The wing is almost entirely missing. Therefore, the receiver location can be important in determining image quality.

We also investigated the possibility of using fewer channels, for receiver location $(-10, 50)$. Figure 10 shows the result of using 13 channels (No. 5, 7, 9, 11, 13, 14, 20, 22, 24, 26, 30, 34, 38) and 9 channels (No. 5, 7, 9, 11, 13, 14, 20, 22, 24). The first row gives the interpolated Fourier data and reconstructed image using 13 channels and the second row is the case for 9 channels. We note that there is some degradation in the interpolated Fourier data and corresponding degradation in the reconstructed image when using 13 channels, but the aircraft still looks recognizable. There is more serious degradation in the image when 9 channels are used.

4. SELECTION OF RECEIVER LOCATION

In last section, the FISC data was available only up to 211.25 MHz and we showed that good images could be formed from this limited data set using 21 or fewer transmitters. Even better images would be possible if full data set from the transmitters could be used. To characterize system performance using full data sets up to 800 MHz, in this section we compute the point spread function (PSF) of the imaging system using the full Fourier data grids from the 21 channels(No. 13, 15, 20, 22, 24, 28, 32, 36, 40, 41, 42, 46, 48, 51, 52, 54, 58, 59, 63, 64, 67, same as those selected in section 2).

As we have seen, for a given flight path, different receiver locations give different sampling patterns in Fourier space, which give image reconstructions with different quality. We suppose the receiver can be placed within a large area. We divide this area into many small cells and compute the sampling pattern and PSF given by the receiver in each cell. We considered the Gaithersburg scenario with the flight path previously defined. In our simulations, the receiver could occupy any location within a $90km$ by $90km$ area, on a rectangular grid with grid spacing $20km$. Figure 11 shows the 24 sampling patterns given by different receiver location at (x_0, y_0) . The radius of the semicircular area in Fourier space is 8.76 radians/meter.

Wide coverage in Fourier space corresponds to a good PSF with a narrow main lobe and small side lobes in the spatial domain. This assumes, however, that the Fourier data is not too sparse. We characterize the quality of a PSF by first normalizing its amplitude and then computing its volume within a $3m$ by $3m$ area surrounding the main lobe. A wider main lobe leads to a larger volume, which is less desirable. Figure 12 shows the PSFs and their volumes, for the 24 sampling patterns shown in Fig. 11. The spatial dimension is $3m$ by $3m$ in each image. We see that receiver location $(50, 10)$ gives the smallest $volume = 44$. Looking at the patterns given in Fig. 11, we see that this receiver location gives wide coverage in Fourier space. We could choose this receiver location and sampling pattern and expect that a useful aircraft image could be formed from the full set of TV data. We mention one additional point, however. The process of DFR from a *nonuniform* grid is a linear, but spatially-varying, operation. Thus, to fully characterize the PSF of the system, it is necessary to examine the responses to point targets located on a dense grid in the spatial domain, not just targets located at the origin, as in Fig. 12.

5. CONCLUSION

We studied a passive multistatic radar imaging problem, where TV signals reflected from an aircraft are collected and used to form an image. The collected data lied on a nonuniform grid in Fourier space. The quality of the Fourier sampling pattern was dependent on the receiver location, for a given flight path. Using FISC, we simulated the bistatic data that could be collected by a passive radar. By selecting a good receiver location, as characterized by the quality of the corresponding Fourier grid, we showed that it is possible to form a useful image of an aircraft via DFR. These results were obtained by using data at low frequencies (below 211.25 MHz). If we had data in the higher frequency range of the UHF band, it would be possible to obtain images with even better quality and resolution. We hope to be able to generate such data with improvements to FISC and our computational capabilities in the future. We also showed how to select a receiver location giving a sampling pattern with good Fourier space coverage

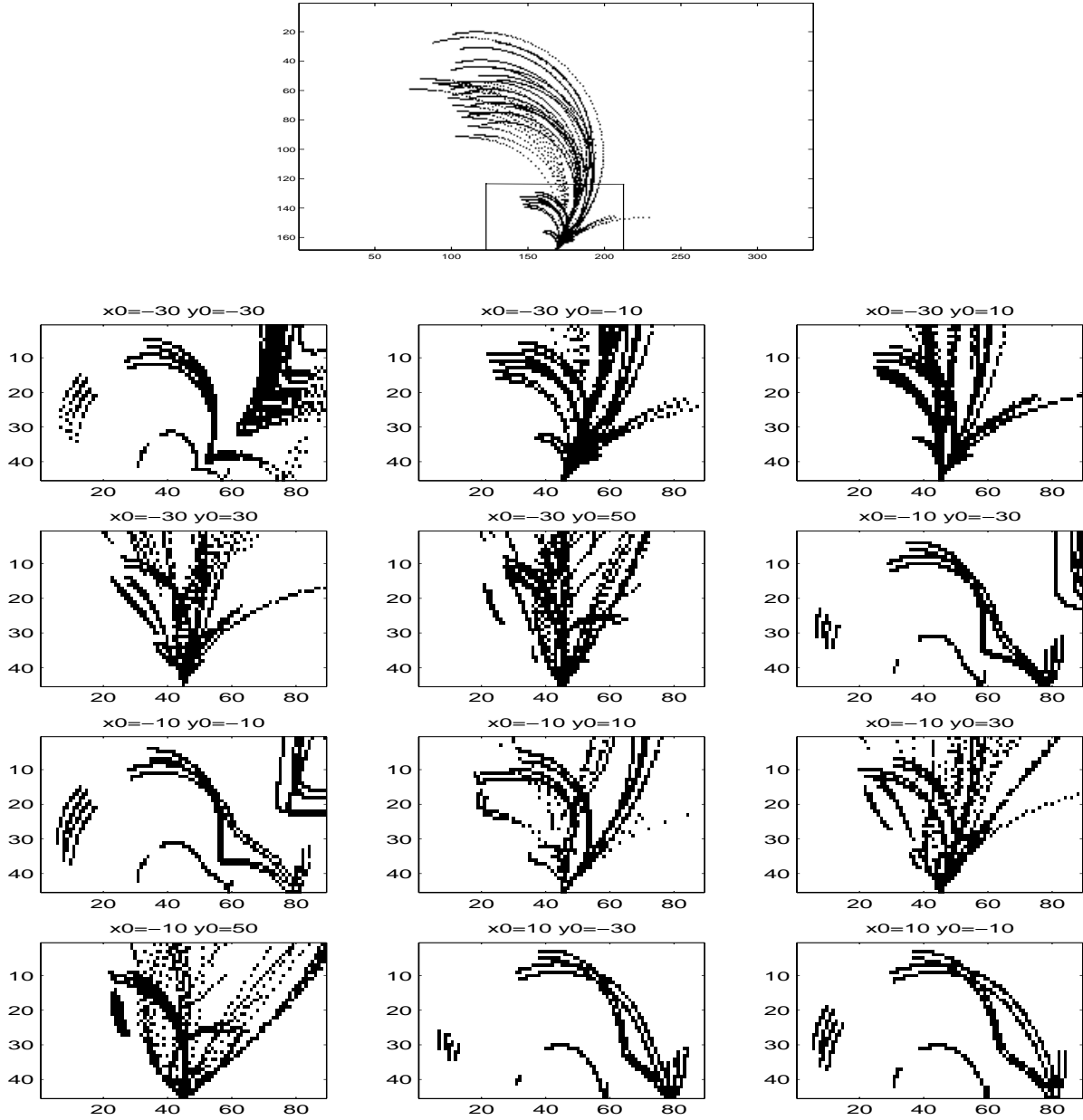


Figure 8. First row: Fourier data sampling pattern for frequencies up to 800 MHz using 21 channels, the smaller rectangular box indicates the bounding box for frequencies up to 211.25 MHz; Second through last rows: different patterns for the simulation (for frequencies up to 211.25 MHz only), at different receiver location.

by comparing PSFs. Our preliminary results suggest that it is possible to form a useful image of an aircraft using a passive radar system operating in the television band.

We note that our FISC data was all generated at a single frequency. In using this data, we essentially assumed that the target reflectivity was invariant to changes in bistatic angle and transmitter frequency. In the future, we plan to do more accurate FISC simulations for all incident/observing angles and the exact transmitting frequencies. As mentioned earlier, we also plan to determine how the shift-invariant PSF changes with target position.

6. ACKNOWLEDGMENT

We thank Dr. Aaron D. Lanterman for generating the FISC data, which was used in our simulations.

REFERENCES

1. H. Griffiths, "Bistatic radar - principles and practice," *SBMO International Microwave Conference/Brazil*, pp. 519–526, Aug 1993.
2. H. Griffiths and N. Long, "Television-based bistatic radar," *IEE Proc., Pt.F* **133**, pp. 649–657, Dec 1986.
3. P. Howland, "Target tracking using television-based bistatic radar," *IEE Proc. -Radar, Sonar Navig.* **146**, pp. 166–174, Jun 1999.
4. <http://silentsentry.external.lmco.com>, "Lockheed Martin Silent Sentry Web page,"
5. D. L. Mensa and G. R. Heidbreder, "Bistatic synthetic-aperture radar imaging of rotating objects," *IEEE Trans. Aerosp Electron Syst.* **18**, pp. 423–431, Jul 1982.
6. O. Arikan and D. Munson, "A tomographic formulation of bistatic synthetic aperture radar," *Proceedings of ComCon 88, Advances in Communications and Control Systems, Baton Rouge, LA*, Oct 19-21 1988.
7. J. L. Walker, "Range-doppler imaging of rotating objects," *IEEE Trans. Aerosp. Electron. Syst.* **AES-16**, pp. 23–52, Jan 1980.
8. C. C. Chen and H. C. Andrews, "Multifrequency imaging of radar turntable data," *IEEE Trans. Aerosp. Electron. Syst.* **AES-16**, pp. 15–22, Jan 1980.
9. D. C. Munson Jr., J. D. O'Brien, and W. K. Jenkins, "A tomographic formulation of spotlight mode synthetic aperture radar," *Proc. IEEE* **71**, pp. 917–925, Aug 1983.
10. J. D. O'Sullivan, "A fast sinc function gridding algorithm for Fourier inversion in computer tomography," *IEEE Trans. Medical Imaging* **4**, pp. 200–207, Dec 1985.
11. V. Rasche, R. Proksa, and et. al., "Resampling of data between arbitrary grids using convolution interpolation," *IEEE Trans. Medical Imaging* **18**, pp. 385–392, May 1999.
12. <http://www.geom.umn.edu/locate/qhull>, "Griddata function and Qhull software Web page at University of Minnesota,"

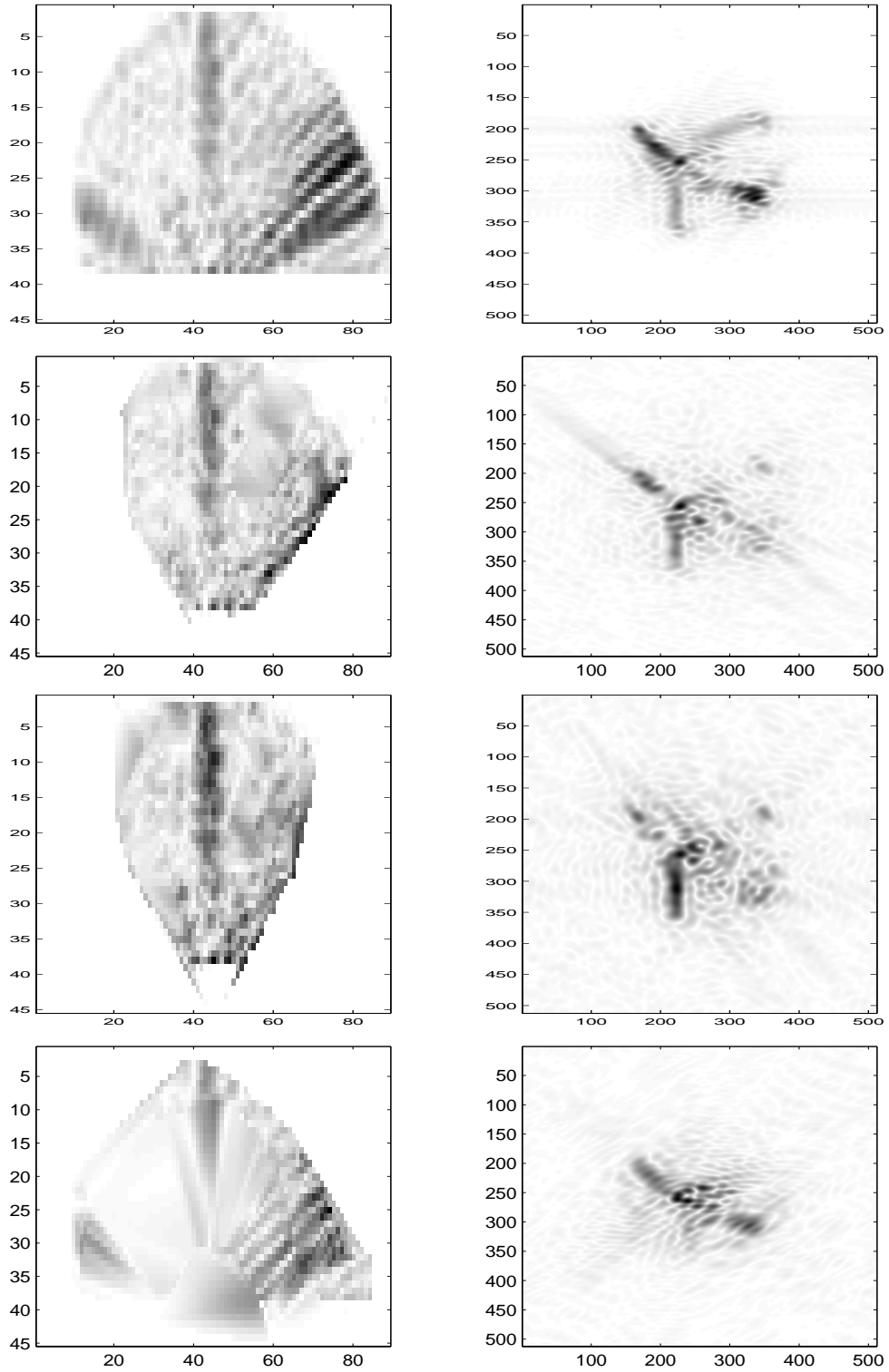


Figure 9. Top: complete Fourier data in a semi-circular area (left), and reconstructed image (right); Second row: interpolated Fourier data from nonuniform grid and reconstructed image, receiver at $(-10, 50)$; Third row: interpolated Fourier data from nonuniform grid and reconstructed image, receiver at $(-30, 50)$; Bottom: interpolated Fourier data from nonuniform grid and reconstructed image, receiver at $(10, -10)$

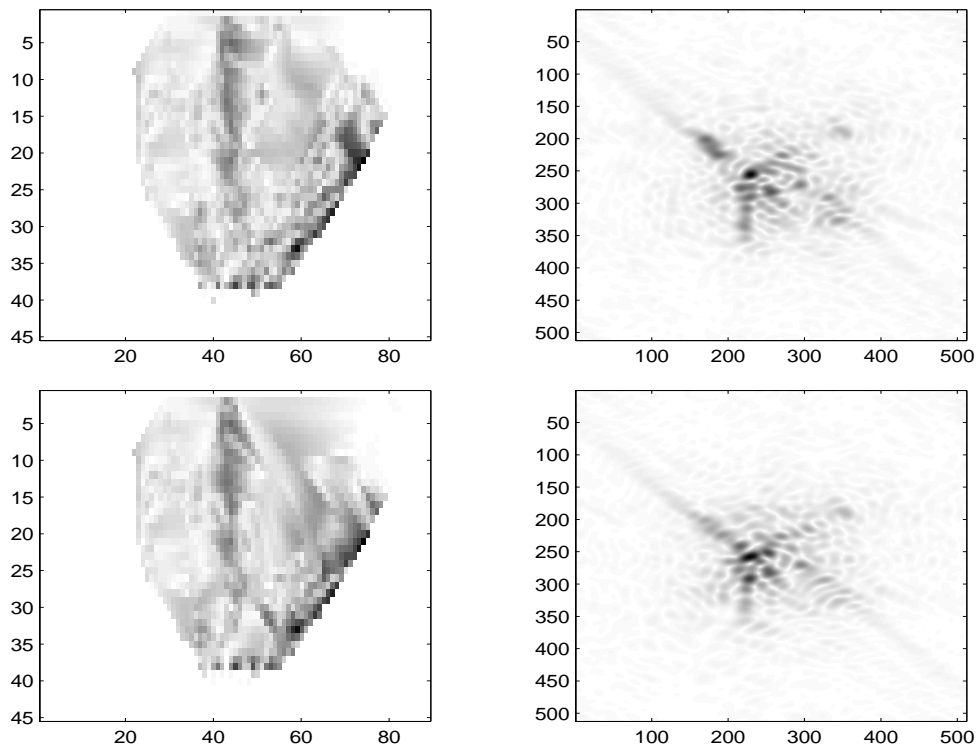


Figure 10. Top: interpolated Fourier data from nonuniform grid and reconstructed image, receiver at $(-10, 50)$, using 13 channels; Bottom: interpolated Fourier data from nonuniform grid and reconstructed image, receiver at $(-10, 50)$, using 9 channels.

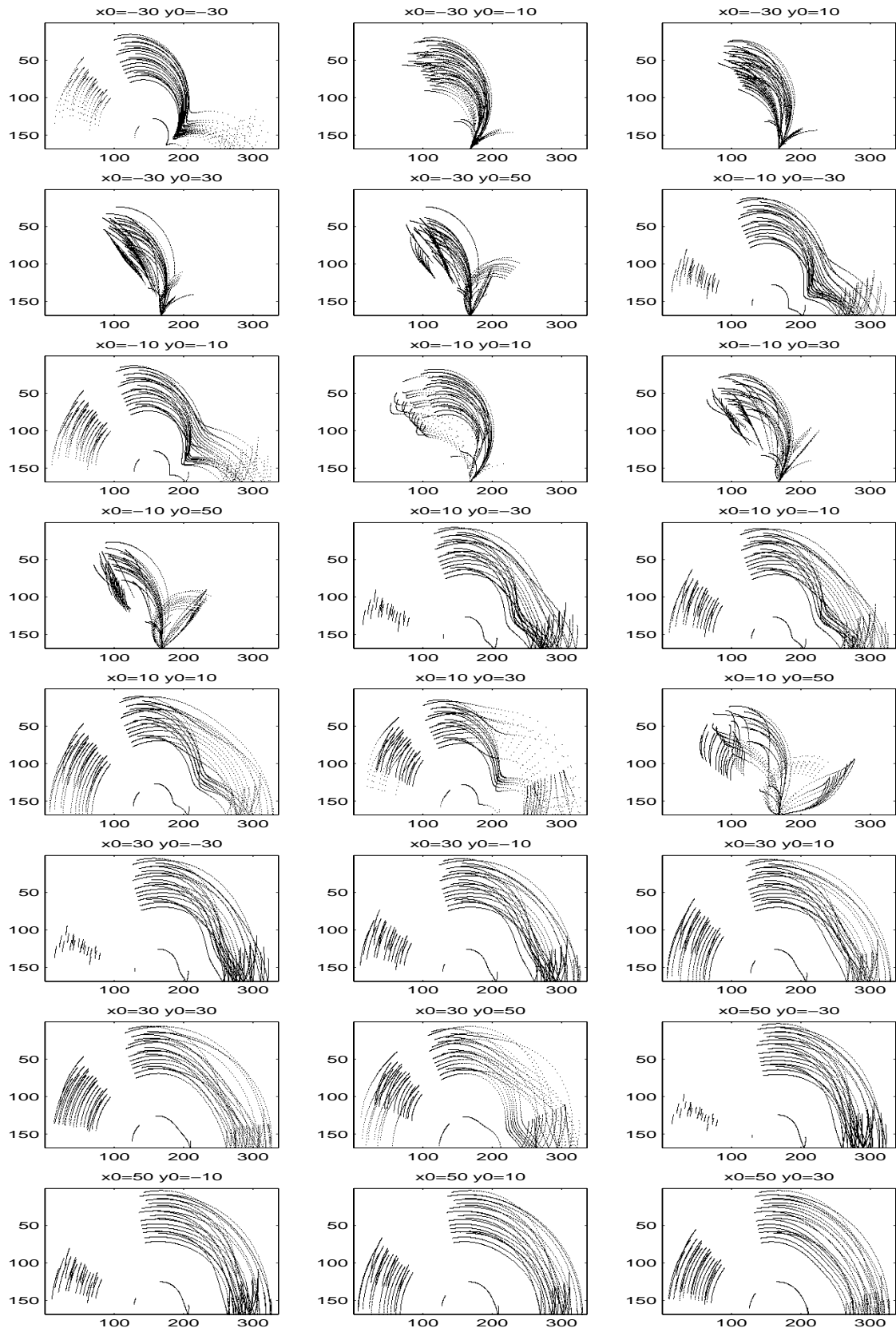


Figure 11. Different Fourier data sampling patterns using 21 channels (for frequencies up to 800 MHz) , for 24 receiver locations (x_0, y_0) .

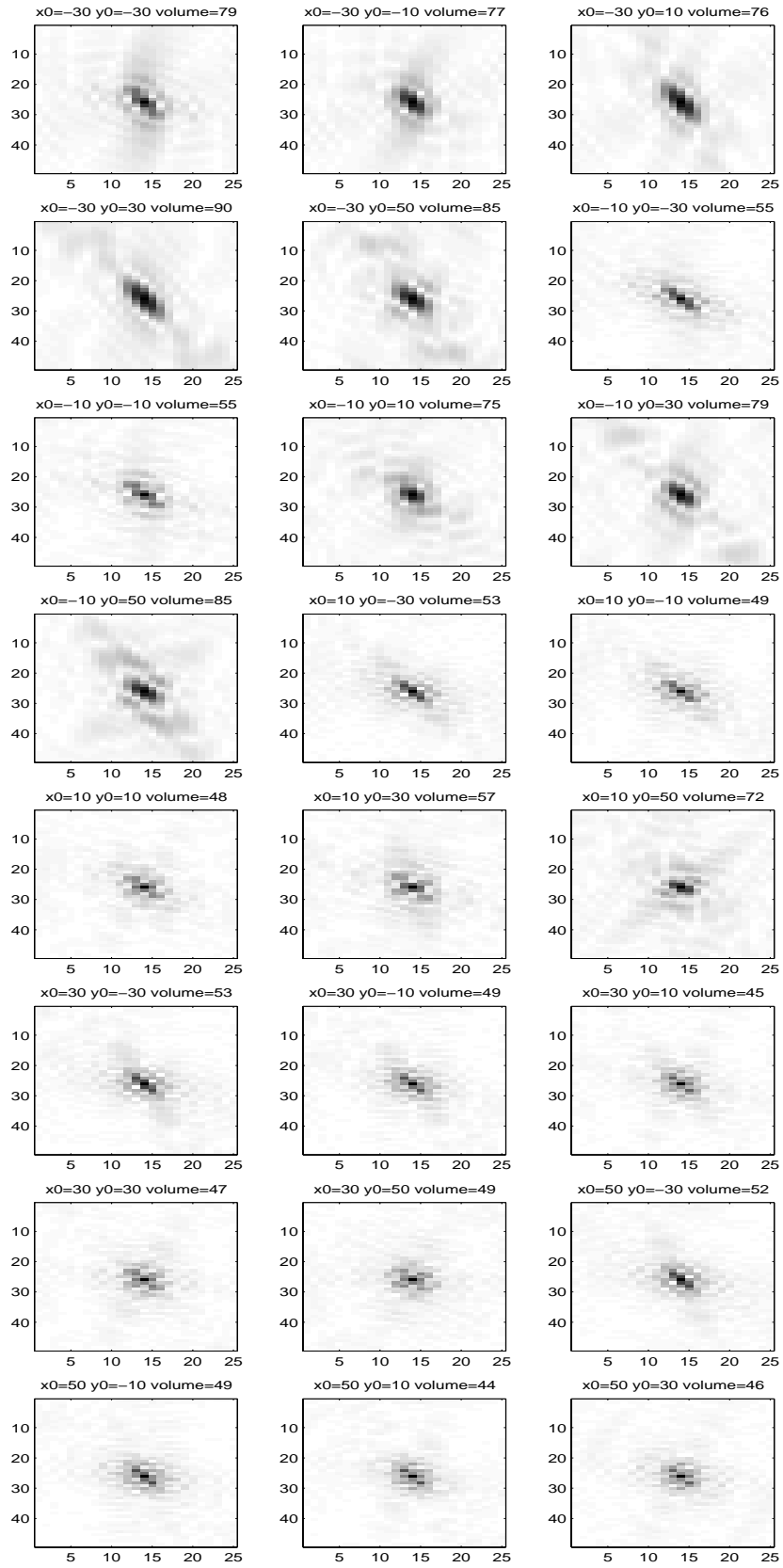


Figure 12. PSF for 24 receiver locations (x_0, y_0) using the selected 21 channels, *volume* is the criterion used to choose the best PSF in this figure.